

Graded index porous optical fibers – dispersion management in terahertz range

Tian Ma,^{1,2} Andrey Markov,^{1,*} Lili Wang,² and Maksim Skorobogatiy¹

¹*École Polytechnique de Montréal, Montreal, Québec H3C3A7, Canada*

²*Xi'an Institute of Optics and Precision Mechanics of CAS, Xi'an, Shannxi 710119, China*

**andrey.markov@polymtl.ca*

Abstract: A graded index porous optical fiber incorporating an air-hole array featuring variable air-hole diameters and inter-hole separations is proposed, fabricated, and characterized in a view of the fiber potential applications in low-loss, low-dispersion terahertz guidance. The proposed fiber features simultaneously low modal and intermodal dispersions, as well as low loss in the terahertz spectral range. We experimentally demonstrate that graded index porous fibers exhibit smaller pulse distortion, larger bandwidth, and higher excitation efficiency when compared to fibers with uniform porosity.

©2015 Optical Society of America

OCIS codes: (040.2235) Far infrared or terahertz; (060.2310) Fiber optics; (260.2030) Dispersion.

References and links

1. L. J. Chen, H. W. Chen, T. F. Kao, J. Y. Lu, and C. K. Sun, "Low-loss subwavelength plastic fiber for terahertz waveguiding," *Opt. Lett.* **31**(3), 308–310 (2006).
2. M. Rozé, B. Ung, A. Mazhorova, M. Walther, and M. Skorobogatiy, "Suspended core subwavelength fibers: towards practical designs for low-loss terahertz guidance," *Opt. Express* **19**(10), 9127–9138 (2011).
3. A. Mazhorova, A. Markov, A. Ng, R. Chinnappan, O. Skorobogata, M. Zourob, and M. Skorobogatiy, "Label-free bacteria detection using evanescent mode of a suspended core terahertz fiber," *Opt. Express* **20**(5), 5344–5355 (2012).
4. A. Hassani, A. Dupuis, and M. Skorobogatiy, "Low loss porous terahertz fibers containing multiple subwavelength holes," *Appl. Phys. Lett.* **92**(7), 071101 (2008).
5. A. Dupuis, J. F. Allard, D. Morris, K. Stoeffler, C. Dubois, and M. Skorobogatiy, "Fabrication and THz loss measurements of porous subwavelength fibers using a directional coupler method," *Opt. Express* **17**(10), 8012–8028 (2009).
6. A. Dupuis, A. Mazhorova, F. Désévéday, M. Rozé, and M. Skorobogatiy, "Spectral characterization of porous dielectric subwavelength THz fibers fabricated using a microstructured molding technique," *Opt. Express* **18**(13), 13813–13828 (2010).
7. S. Atakaramians, S. Afshar, B. M. Fisher, D. Abbott, and T. M. Monroe, "Low loss, low dispersion and highly birefringent terahertz porous fibers," *Opt. Commun.* **282**(1), 36–38 (2009).
8. M. Skorobogatiy, *Nanostructured and Subwavelength Waveguides* (Wiley, 2012).
9. S. Atakaramians, S. Afshar, B. M. Fischer, D. Abbott, and T. M. Monroe, "Porous fibers: a novel approach to low loss THz waveguides," *Opt. Express* **16**(12), 8845–8854 (2008).
10. K. Nielsen, H. K. Rasmussen, P. U. Jepsen, and O. Bang, "Porous-core honeycomb bandgap THz fiber," *Opt. Lett.* **36**(5), 666–668 (2011).
11. S. Atakaramians, S. Afshar, T. M. Monroe, and D. Abbott, "Terahertz dielectric waveguides," *Adv. Opt. Photon.* **5**(2), 169–215 (2013).
12. B. Bowden, J. A. Harrington, and O. Mitrofanov, "Silver/polystyrene-coated hollow glass waveguides for the transmission of terahertz radiation," *Opt. Lett.* **32**(20), 2945–2947 (2007).
13. T. Ito, Y. Matsuura, M. Miyagi, H. Minamide, and H. Ito, "Flexible terahertz fiber optics with low bend-induced," *J. Opt. Soc. Am. B* **24**(5), 1230–1235 (2007).
14. A. Dupuis, K. Stoeffler, B. Ung, C. Dubois, and M. Skorobogatiy, "Transmission measurements of hollow-core THz Bragg fibers," *J. Opt. Soc. Am. B* **28**(4), 896–907 (2011).
15. M. Skorobogatiy and A. Dupuis, "Ferroelectric all-polymer hollow Bragg fibers for terahertz guidance," *Appl. Phys. Lett.* **90**(11), 113514 (2007).
16. M. Cho, J. Kim, H. Park, Y. Han, K. Moon, E. Jung, and H. Han, "Highly birefringent terahertz polarization maintaining plastic photonic crystal fibers," *Opt. Express* **16**(1), 7–12 (2008).

17. H. Han, H. Park, M. Cho, and J. Kim, "Terahertz pulse propagation in a plastic photonic crystal fiber," *Appl. Phys. Lett.* **80**(15), 2634 (2002).
18. B. Bowden, J. A. Harrington, and O. Mitrofanov, "Fabrication of terahertz hollow-glass metallic waveguide with inner dielectric coatings," *Appl. Phys. Lett.* **104**, 093110 (2008).
19. O. Mitrofanov and J. A. Harrington, "Dielectric-lined cylindrical metallic THz waveguides: mode structure and dispersion," *Opt. Express* **18**(3), 1898–1903 (2010).
20. X. L. Tang, Y. W. Shi, Y. Matsuura, K. Iwai, and M. Miyagi, "Transmission characteristics of terahertz hollow fiber with an absorptive dielectric inner-coating film," *Opt. Lett.* **34**(14), 2231–2233 (2009).
21. A. Markov and M. Skorobogatiy, "Two-wire terahertz fibers with porous dielectric support," *Opt. Express* **21**(10), 12728–12743 (2013).
22. A. Markov and M. Skorobogatiy, "Hybrid plasmonic terahertz fibers for sensing applications," *Appl. Phys. Lett.* **103**(18), 181118 (2013).
23. A. Markov, H. Guerboukha, and M. Skorobogatiy, "Hybrid metal wire-dielectric terahertz waveguides: challenges and opportunities," *J. Opt. Soc. Am. B* **31**, 2587–2600 (2014).
24. J. Anthony, R. Leonhardt, and A. Argyros, "Hybrid hollow core fibers with embedded wires as THz waveguides," *Opt. Express* **21**(3), 2903–2912 (2013).
25. M. Skorobogatiy, K. Saitoh, and M. Koshiba, "Full-vectorial coupled mode theory for the evaluation of macro-bending loss in multimode fibers. application to the hollow-core photonic bandgap fibers," *Opt. Express* **16**(19), 14945–14953 (2008).
26. A. Hassani, A. Dupuis, and M. Skorobogatiy, "Porous polymer fibers for low-loss Terahertz guiding," *Opt. Express* **16**(9), 6340–6351 (2008).
27. K. Nielsen, H. K. Rasmussen, A. J. Adam, P. C. Planken, O. Bang, and P. U. Jepsen, "Bendable, low-loss Topas fibers for the terahertz frequency range," *Opt. Express* **17**(10), 8592–8601 (2009).
28. J. Anthony, R. Leonhardt, A. Argyros, and M. Large, "Characterization of a microstructured Zeonex terahertz fiber," *J. Opt. Soc. Am. B* **28**(5), 1013–1018 (2011).
29. M. Cvijetic and I. B. Djordjevic, *Advanced Optical Communication Systems and Networks* (Arctech House, 2013).
30. I. P. Kaminow, T. Li, and A. E. Willner, *Optical Fiber Telecommunications Volume VIA: Components and Subsystems*, 6th ed., (Academic Press, 2013).
31. G. Fiol, J. A. Lott, N. N. Ledentsov, and D. Bimberg, "Multimode optical fibre communication at 25 Gbit/s over 300 m with small spectral-width 850 nm VCSELS," *Electron. Lett.* **47**(14), 810–811 (2011).
32. J. D. Downie, J. E. Hurley, D. V. Kuksenkov, C. M. Lynn, A. E. Korolev, and V. N. Nazarov, "Transmission of 112 Gb/s PM-QPSK signals over up to 635 km of multimode optical fiber," *Opt. Express* **19**(26), B363–B369 (2011).
33. G. P. Agrawal, *Fiber-optic Communication Systems*, 3rd ed., (Wiley, 2002).
34. Y. Akimoto, M. Asai, K. Koike, K. Makino, and Y. Koike, "Poly(styrene)-based graded-index plastic optical fiber for home networks," *Opt. Lett.* **37**(11), 1853–1855 (2012).
35. K. Makino, T. Kado, A. Inoue, and Y. Koike, "Low loss graded index polymer optical fiber with high stability under damp heat conditions," *Opt. Express* **20**(12), 12893–12898 (2012).
36. R. Kruglov, S. Loquai, C. A. Bunge, O. Ziemann, B. Schmauss, and J. Vinogradov, "10 Gbit/s short-reach transmission over 35 m large-core graded-index polymer optical fiber," *Optical Fiber Communication Conference and Exposition (OFC/NFOEC)*, 2011, p 1–3.
37. M. A. Illarramendi, J. Arrue, I. Ayesta, F. Jiménez, J. Zubia, I. Bikandi, A. Tagaya, and Y. Koike, "Amplified spontaneous emission in graded-index polymer optical fibers: theory and experiment," *Opt. Express* **21**(20), 24254–24266 (2013).
38. D. S. Montero and C. Vázquez, "Analysis of the electric field propagation method: theoretical model applied to perfluorinated graded-index polymer optical fiber links," *Opt. Lett.* **36**(20), 4116–4118 (2011).
39. R. Lwin, G. Barton, L. Harvey, J. Harvey, D. Hirst, S. Manos, M. C. J. Large, L. Poladian, A. Bachmann, H. Poisel, and K.-F. Klein, "Beyond the bandwidth-length product: Graded index microstructured polymer optical fiber," *Appl. Phys. Lett.* **91**(19), 191119 (2007).
40. M. A. Eijkelenborg, A. Argyros, A. Bachmann, G. Barton, M. C. J. Large, G. Henry, N. A. Issa, K. F. Klein, H. Poisel, W. Pok, L. Poladian, S. Manos, and J. Zagari, "Bandwidth and loss measurements of graded-index microstructured polymer optical fibre," *Electron. Lett.* **40**(10), 592–593 (2004).
41. B. Ung, A. Mazhorova, A. Dupuis, M. Rozé, and M. Skorobogatiy, "Polymer microstructured optical fibers for terahertz wave guiding," *Opt. Express* **19**(26), B848–B861 (2011).
42. M. Skorobogatiy and J. Yang, *Fundamentals of Photonic Crystal Guiding* (Cambridge University, 2009).
43. A. Markov, A. Mazhorova, and M. Skorobogatiy, "Planar Porous THz Waveguides for Low-Loss Guidance and Sensing Applications," *IEEE Transactions on Terahertz Science and Technology* **3**(1), 96–102 (2013).
44. M. Skorobogatiy and N. Guo, "Bandwidth enhancement by differential mode attenuation in multimode photonic crystal Bragg fibers," *Opt. Lett.* **32**(8), 900–902 (2007).

1. Introduction

The terahertz frequency range has strong potential for various technological and scientific applications, such as sensing, imaging, communications, and spectroscopy. However, most

terahertz (THz) sources are immobile, thus designing efficient THz waveguides for flexible delivery of the broadband THz radiation is an important step towards practical applications of terahertz techniques. Moreover, THz waveguides can be very useful on the system integration level when used for connectorization of the diverse THz point devices, such as sources, filters, sensor cells, detectors, etc. Availability of the THz fibers is also crucial for various niche applications such as endoscopy and crevice inspection.

The main complexity in designing terahertz fibers is the fact that almost all materials are highly absorbent (over ~ 1 m propagation) in the THz spectral range. A traditional way of guiding light would be to use solid-core fibers, such as step index core/clad fibers, or solid-core microstructured fibers. In these fibers, however, the fraction of light guided in the solid core is significant, and, therefore, fiber transmission loss is typically close to the absorption loss of the core material. For completeness we mention that in the 0.1-1 THz spectral range, amorphous materials suitable for fiber drawing (such as glasses and polymers) have losses that are typically higher than $0.1\text{--}0.3\text{ cm}^{-1}$.

In order to break away from the loss limit imposed by the fiber material absorption, subwavelength [1–3], porous [4–11], and hollow core THz fibers of various types [11–15] were introduced. The lowest absorption loss occurs in dry gases, therefore transmission losses of the THz fibers can be reduced significantly below the loss of the fiber core material by maximizing the fraction of the THz power guided in the low-loss gas. Using this strategy, very low transmission losses in the range of 0.01 cm^{-1} were demonstrated using the abovementioned fibers.

In particular, hollow core fibers are of great interest as they also tend to offer broadband guidance. Among such fibers one has to distinguish between dielectric photonic crystal fibers [16,17], metallized capillary fibers [18–20], and hybrid metal/dielectric fibers [21–24]. However, dielectric photonic crystal fibers and metallized capillaries require the use of relatively large core diameters in order to keep the propagation loss low. Therefore, such fibers operate mostly in the multimode or in the few-mode regime. In contrast, hybrid metal/dielectric fibers, which are essentially two wire waveguides surrounded by a porous dielectric cladding, operate in a single mode regime. On the same note, design of such fibers is challenging due to ease of parasitic excitation of the cladding modes, and it still remains to be seen if such fibers can show losses comparable to that of other hollow-core fibers.

Therefore, if the goal is to guide THz light over distances of ~ 1 m in a single mode regime with losses on the order of 0.01 cm^{-1} , then the only choices that are currently available are either using a subwavelength or porous fiber. When comparing porous and subwavelength fibers [1–9] it was found that porous fibers are generally superior to the rod-in-the-air subwavelength fibers as porous fibers offer larger bandwidth [6] and lower bending loss [25,26].

Another complication when guiding broadband THz pulses is the effect of group velocity dispersion on the pulse shape. In fact, waveguide modes typically exhibit significant variation of their optical properties as a function of frequency (refractive index, group velocities, etc.), thus leading to pulse broadening, and hence, signal amplitude reduction. Consequently, waveguide dispersion management is an important issue when guiding broadband pulses. Dispersion optimized single mode THz fibers have been first studied in [6, 27,28]. Particularly, in [27,28] the authors used solid core microstructured fibers with optimized geometrical parameters to minimize group velocity dispersion of the fiber fundamental mode in the 0.2-1.2 THz frequency range. Dispersion of the fundamental mode was optimized to be less than $1\text{ ps}/(\text{THz}\cdot\text{cm})$ in the whole THz frequency range. However, due to guidance in the solid core, losses of such fibers were comparable to that of the bulk absorption loss of the fiber material $\sim 0.1\text{--}0.5\text{ cm}^{-1}$ (increasing towards higher frequencies). In [6], the authors studied dispersion and losses of the porous fibers and they have concluded that losses in such fibers could be significantly reduced below that of the core material loss by introducing porosity into the fiber core. At the same time, the authors of [6,27,28] have observed that both

in solid core and porous fibers, group velocity dispersion can be very large at low frequencies due to rapid change in the modal confinement, while dispersion can decrease by more than an order of magnitude at higher frequencies (strong confinement limit). At higher frequencies, however, the fiber can become multimode and one has to worry about the effect of the intermodal dispersion.

Therefore, we conclude that when designing broadband dielectric fibers for THz guidance one must consider several trade-offs between dispersion, loss and single mode versus multimode operation. In order to demonstrate the nature of these trade-offs we consider guidance in the rod-in-the-air fiber of radius a having core and cladding refractive indices ϵ_c and ϵ_a respectively. In our analysis we divide the whole frequency range into 3 spectral regions as shown in Fig. 1. In the first region $\omega < \omega_0 \sim c / (a \cdot \sqrt{\epsilon_c - \epsilon_a})$ the fiber is single mode and it guides in the weak localization regime. At these low frequencies one often calls the fiber a “subwavelength” fiber. In this regime, modal losses are much lower than the bulk absorption losses of the core material as a significant fraction of the modal fields is found outside of the fiber core and in the low-loss air cladding. In this regime, modal group velocity dispersion is also low as the mode is mostly guided in air. At the same time, macro-bending losses in this subwavelength guidance regime are very high as modal effective refractive index is very close to that of air, which typically renders subwavelength fibers unusable at frequencies significantly lower than ω_0 .

Next, we consider the second region $\omega_0 < \omega < \omega_{sm}$, where ω_{sm} is a cutoff frequency of the second order mode. In this frequency range the fiber is still single mode. Note that ω_{sm} and ω_0 are simply proportional to each other $\omega_{sm} \sim 2-4 \cdot \omega_0$ with a proportionality coefficient dependent on the symmetry of the second order mode that can be excited by a given THz source. In the vicinity of ω_0 the mode localization changes dramatically from a weak to strong localisation in the fiber core. This transition leads to a fast increase in the value of the modal refractive index, followed by a significant increase in the modal loss and modal group velocity dispersion. When increasing the operation frequency towards ω_{sm} , one observes a monotonic increase in the modal loss, which approaches that of the core material. Furthermore, modal group velocity dispersion decreases significantly as the modal effective refractive index becomes virtually constant and close to that of the core refractive index. Additionally, at these higher frequencies macro-bending loss decreases dramatically due to improved modal confinement in the fiber core. So far, most of the experimental demonstrations of THz guiding were performed in this spectral range. It was clearly identified that high dispersion at lower frequencies and high propagation loss at higher frequencies present major challenges in the design of a solid-core THz fiber.

In principle, high modal loss at higher frequencies can be mitigated by using porous fibers with deeply subwavelength core size. In this case, absorption loss of the porous core can be made significantly lower than that of the constituent solid material. Additionally, modal group velocity dispersion decreases with lower refractive index contrast between the fiber core and cladding materials. Thus, using porous fibers can help in reducing both loss and group velocity dispersion of the fundamental mode.

Even when using porous materials in the fiber core, the fundamental limitation on the usable bandwidth is given by $\omega_0 < \omega < \omega_{sm}$ where, as mentioned earlier, $\omega_{sm} \sim 2-4 \cdot \omega_0$ in the rod-in-the-air fibers. This frequency range is quite limited as it spans less than an octave. The question then is how to extend the usable bandwidth of THz fibers. There are two approaches that one can pursue. One is designing microstructured fibers with an extended range of single mode operation. The other one is accepting multimode guidance, while at the same time optimizing fiber performance over an ensemble of the guided modes.

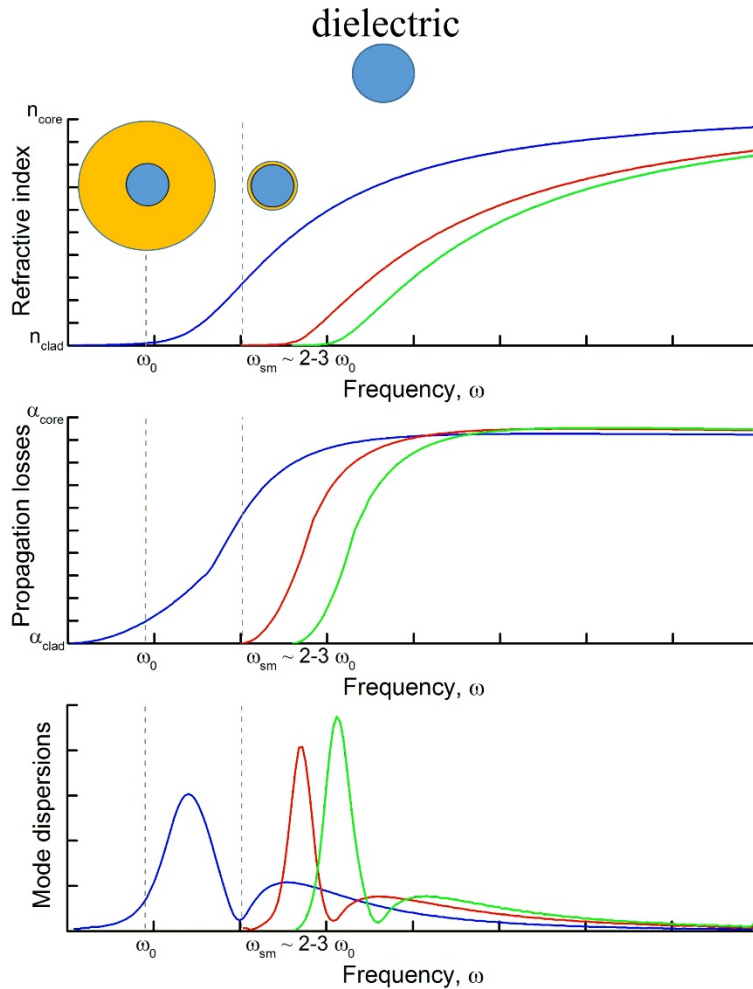


Fig. 1. Modal propagation properties of the dielectric THz fibers. Blue lines correspond to the fundamental mode of the fiber, red and green lines – to higher order modes.

Multimode fibers (MMFs) offer several general advantages over single mode fibers such as high coupling efficiency and broadband operation. Moreover, in the multimode regime, most of the lower order modes show strong confinement in the fiber core, and, therefore, MMFs typically feature low modal group velocity dispersion, and low bending loss. As mentioned earlier, even at high frequencies modal absorption can be made significantly lower than absorption loss of the fiber core material by introducing subwavelength porosity into the fiber core. Moreover, a new phenomenon called intermodal dispersion has to be taken into account when considering THz pulse propagation in the multimode fibers. Simply speaking, an incoming pulse at the fiber input is split between several fiber modes. If the group velocities of the guided modes are somewhat different from each other, then various copies of the original pulse will arrive at the fiber output at different times, thus causing pulse shape degradation. In addition, when looking at a particular fiber mode, the shape of the pulse carried by such a mode will be additionally affected by this mode group velocity dispersion. Therefore, reduction of both the modal and the intermodal dispersions presents an important problem when designing multimode THz fibers.

To date, multimode fibers have been exhaustively researched in the context of their application in short-length high bit-rate communication systems operating in the visible

spectral range [29–32]. In such systems, fiber communication bandwidth is limited by the intersymbol interference caused by the intermodal dispersion, which arises because of the diverse group velocities of the individual fiber modes [33]. To address the issue of intermodal dispersion, graded index polymer optical fibers (GI-POF) have been extensively studied since the 1990s [34–40]. In such fibers, the core refractive index decreases from its maximal value at the core center as a certain power (~ 2) of the distance. As a result, intermodal group velocity dispersion can be dramatically reduced. In practice, in order to realize variable refractive index profiles in the fiber core one either uses a non-uniform distribution of dopants or a non-uniform distribution of geometrical features (such as holes). Thus, Y. Akimoto et al. [34] reported the fabrication and experimental investigation of the doped PSt-based GI-POFs. The graded refractive index distribution was achieved by controlling the radial dopant concentration. The authors confirmed that this fiber has a high bandwidth (4.4 GHz at 655 nm with fiber length of 50 m) and low attenuation (166–193 dB/km at 670–680 nm) and can be used for home networks. In [39], R. Lwin et al. reported another type of graded index fiber with graded index profile obtained by porous cladding with specially designed air hole positions and diameters, namely graded index microstructured polymer optical fibers (GI-mPOF). They demonstrated experimentally that the bandwidths of the proposed GI-mPOFs were much wider than those of the commercial GI-POF.

When designing multimode fibers for delivery of THz pulses we adopt the manufacturing strategy of graded index refractive index profiles using non uniform distribution of holes in the fiber core. However, when simply trying to scale the GI-mPOF design presented in [39] to THz wavelengths, the outer diameter of the resultant THz fiber becomes close to 5–10 cm, which is not practical. In fact, GI-mPOF presented in [39] does not contain subwavelength features (air holes), therefore the core material does not operate in the effective medium regime. Instead, the features are comparable or larger than the wavelength of light, and their size and position are optimized in order to provide a certain resonant response of the microstructured cladding. As a consequence, the diameter of such graded index fibers is in hundreds of wavelengths for which they are designed, and obviously scaling of these fibers to THz will be impractical. Moreover, the GI-mPOFs developed for communications in the visible/near-IR have to operate in a very narrow spectral range as the signal bandwidth (~ 10 GHz) to the carrier frequency ($\sim 10^{14}$ Hz) ratio is $\sim 10^{-4}$, whereas for THz GI-mPOFs this ratio is close to 1.

In this paper, we propose a novel graded index porous optical fiber which is specifically designed for applications in the terahertz spectral range (THz GI-POF). The fiber is made from polyethylene plastic and features a non-uniform array of the variable size subwavelength holes positioned at subwavelength separations with respect to each other, thus resulting in a graded refractive index effective medium. The outer diameter of the fiber is ~ 1.4 mm, which is at most 7 times larger than the wavelength of operation in the whole 0.2–1.5 THz operation range. The fiber is single mode below 0.35 THz, while at higher frequencies it operates in a few-mode regime. Due to high porosity, fiber absorption loss is only a fraction of the bulk absorption loss of polyethylene, and in the whole operation range it varies from 0.025 cm^{-1} at 0.3 THz to 0.15 cm^{-1} at 1.5 THz. Modal group velocity dispersions of the individual modes is reduced below $1 \text{ ps}/(\text{THz}\cdot\text{cm})$ in the whole operational range due to the use of porous materials and due to the relatively large core size. At the same time, intermodal dispersion is reduced below $2 \text{ ps}/(\text{THz}\cdot\text{cm})$ due to the choice of the graded index profile. Finally, we confirm experimentally and numerically that THz-GI-POFs have considerably superior optical properties when compared to regular THz porous optical fibers that feature similar geometrical dimensions, however only use a uniform array of holes. We believe that graded index porous optical fibers offer a clear pathway towards designing low-loss, broadband, low dispersion fibers for THz frequency range.

2. Fiber design and fabrication

In order to obtain a graded index profile similar to that of the conventional GI-POFs (see, for example Ref [34].) we use a hexagonal lattice of 5 rings of air-holes with gradually varied air-hole diameters and inter-hole separations [as shown in Fig. 2(a)]. In our design, the azimuthal average refractive index was approximated by the following power law:

$$n(r) = n_0(1 - a(r/R)^g)^{1/2} \quad (1)$$

where a is a constant which determines the index profile of the designed fiber, R is the radius of this fiber. In the case of porous fibers, local value of the core refractive index is determined by the local value of the air filling fraction $f(r)$. Therefore, in order to design porous fiber geometry we have to first find the radially dependent air filling fraction $f(r)$ that results in the desired graded index profile given by Eq. (1). As detailed in [8], dielectric properties of the porous core can be described using an anisotropic dielectric permittivity tensor. Moreover, at higher frequencies, when transverse modal electric fields become much larger than the modal longitudinal electric fields, impact of anisotropy becomes small. In this regime, one can consider dielectric constant of the porous core material to be that of a transverse component of the dielectric tensor:

$$\epsilon(r) = n(r)^2 = \sqrt{\left(\frac{1}{2} - f\right)^2 \cdot \Delta\epsilon^2 + \epsilon_a \epsilon_p + \left(\frac{1}{2} - f\right) \cdot \Delta\epsilon} \quad (2)$$

where ϵ_a and ϵ_p are the dielectric constants of the air and the used polymer, respectively, and $\Delta\epsilon = \epsilon_p - \epsilon_a$. Now, using Eqs. (1) and (2), we can find the distribution of the air filling fraction $f(r)$ that results in the graded index profile given by Eq. (1). In our simulations we have used $g = 2$ and $a = 0.2$. Finally, using the expression for $f(r)$ at the air-hole center, we can extract the relation between the local value of the hole diameter d and the inter-hole separation Λ , which can be given as

$$f(r) = \frac{\pi}{2\sqrt{3}} \frac{d^2}{\Lambda^2} \quad (3)$$

The theoretical index distribution used in our simulation is depicted in Fig. 2(b).

All fibers presented in this paper were fabricated using commercial rods of low density polyethylene (LDPE) known as one of the lowest absorptive polymers in the THz region [41]. The fiber preforms were fabricated using the drilling method. The air-hole arrays with designed structural parameters were drilled on the transversal surface of LDPE rods with an outer diameter of 1.5 inches and a length of 12 cm. Then the fabricated preforms were drawn down to fibers with an outer diameter (OD) of 1.3-1.5 mm in a fiber drawing tower. In order to make a reference measurement, a porous optical fiber with uniform diameters and inter-hole separations comparable to those of the GI-mPOF was also fabricated using the same material and fabrication technique. The cross sections of the two fibers are shown in Fig. 2(c) and 2(d), respectively. The air filling fraction of fabricated GI-mPOF and mPOF are 43.3% and 43.0%.

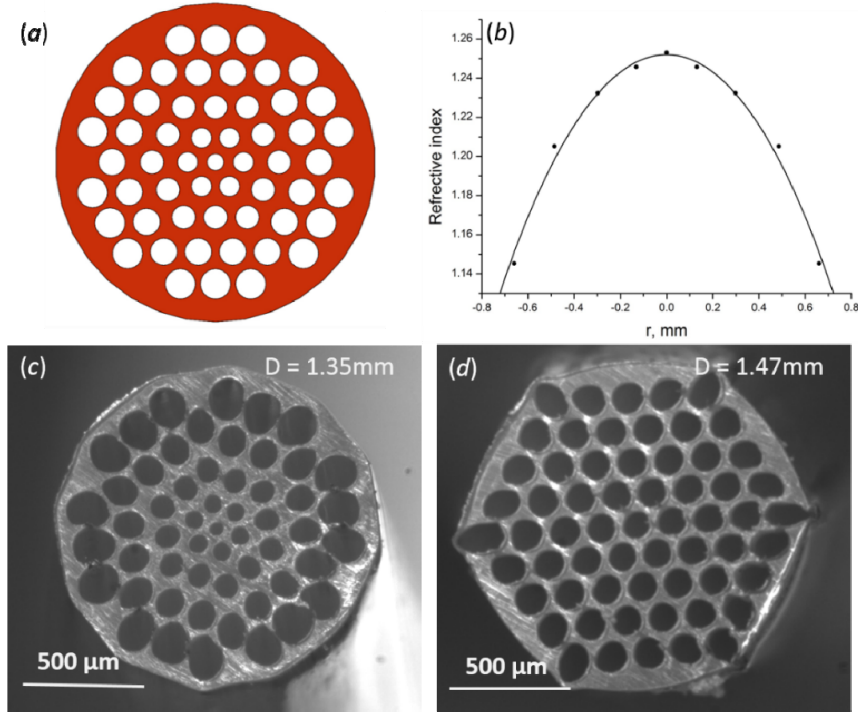


Fig. 2. (a) The schematic representation and (b) the theoretical index profile of the designed GI-mPOF. The dots correspond to the localized refractive index at each layer, while the solid line is the theoretical index profile calculated using Eq. (2). The cross-sections of (c) GI-mPOF (outer diameter OD = 1.35mm) and (d) mPOF (OD = 1.47mm)

3. Numerical model and simulation results

To investigate the optical properties of the proposed GI-mPOF numerically, we used the commercial software COMSOL to solve for the complex effective index and field distribution of the guided modes. Figure 3 shows the calculated modal refractive index (n_{mod}) and group velocities (v_g) of the guided modes for the two fibers. In these figures, the dots' colors represent the logarithmic flux coupling coefficient (C_m^2). In the group velocity versus frequency graph we notice that the variation of the values of group velocities is smaller for the case of the GI-mPOF.

Correspondingly, the normalized amplitude coupling coefficient C_m is computed from the overlap integral of the respective flux distribution of the m -th mode with that of the 2D Gaussian beam used as a source. Specifically, the definition of C_m is based on the continuity of the transverse field components across the input interface (i.e. cross-section of the fibers) between the incident beam and the excited fiber modes [42, 43]:

$$C_m = \frac{1}{4} \int dx dy (\mathbf{E}_m^*(x, y) \times \mathbf{H}_{\text{input}}(x, y) + \mathbf{E}_{\text{input}}(x, y) \times \mathbf{H}_m^*(x, y)) \times \frac{1}{\sqrt{\frac{1}{2} \text{Re} \int dx dy (\mathbf{E}_{\text{input}}^*(x, y) \times \mathbf{H}_{\text{input}}(x, y))} \times \sqrt{\frac{1}{2} \text{Re} \int dx dy (\mathbf{E}_m^*(x, y) \times \mathbf{H}_m(x, y))}} \quad (4)$$

To model the field structure of the source, we assume an x-polarized 2D Gaussian beam whose fields are normalized to carry power P , then limited by an aperture of radius R as follows:

$$\begin{aligned}\vec{E}_{Input}(x, y) &= \vec{x} \cdot \sqrt{\frac{2P}{\pi\sigma^2}} \cdot \exp\left[-\frac{y^2}{2\sigma^2}\right] \\ \vec{H}_{Input}(x, y) &= \vec{y} \cdot \frac{1}{\sqrt{\mu_0/\epsilon_0}} \cdot \sqrt{\frac{2P}{\pi\sigma^2}} \cdot \exp\left[-\frac{y^2}{2\sigma^2}\right], \text{ for } x^2 + y^2 \leq R^2; \\ \vec{E}_{Input}(x, y) &= 0, \vec{H}_{Input}(x, y) = 0, \text{ for } x^2 + y^2 > R^2.\end{aligned}\quad (5)$$

where the Gaussian beam waist parameter σ is related to the full-width half-maxima by field as $FWHM = 2\sigma\sqrt{2\ln 2}$, \vec{x} and \vec{y} are the unit vectors in x- and y-directions, $\sqrt{\mu_0/\epsilon_0}$ is the intrinsic impedance of vacuum, and R is equal to the radius of the fiber (~ 0.65 mm). The frequency dependence of the beam waist was measured experimentally and then fitted by a linear function of the input wavelength $\sigma = 0.96\lambda + 1.4\text{mm}$.

As shown in Fig. 4, the fundamental mode of the GI-mPOF (shown as the blue curve) is predominantly excited in the entire frequency range, whereas coupling into higher order modes is correspondingly lower as opposed to the fiber with uniform holes. In the case of traditional mPOF, higher order modes have higher coupling coefficients compared to the fundamental mode (black curve) above 0.7 THz.

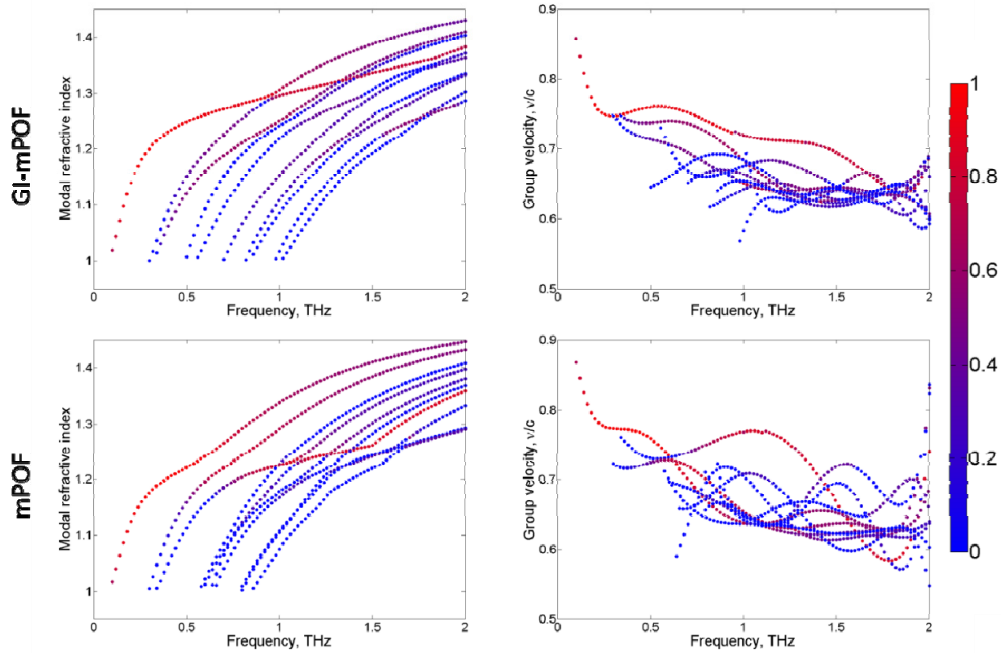


Fig. 3. (a) The modal refractive indices and (b) the group velocities of the proposed GI-mPOF and the traditional mPOF. The dots' colors represent the logarithmic flux coupling coefficient of each mode at the given frequency.

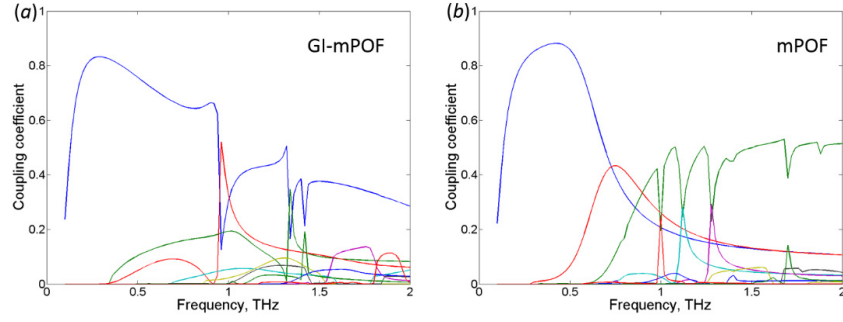


Fig. 4. The coupling efficiency by power for the proposed GI-mPOF and the traditional mPOF

Based on the modal refractive indices and group velocity, we calculated the individual mode (or waveguide) dispersion ($\sqrt{\langle D^2 \rangle}$) and the intermodal dispersion ($\sqrt{\langle \Delta v_g^{-2} \rangle}$). The waveguide dispersion was computed based on the first order derivative of the modal propagation constant. The intermodal dispersion was defined as the standard deviation of the modal delay and can be given as [44]:

$$\langle \Delta v_g^{-2} \rangle = \langle v_g^{-2} \rangle - \langle \Delta v_g^{-1} \rangle^{-2} \quad (6)$$

where $\langle M \rangle$ denotes the average of the variable M and is defined as $\langle M \rangle = \sum_j M_j C_j^2$.

Assuming pulse intensity is given by $I(t, 0) \sim \exp(-(\frac{2t}{\tau_0})^2)$ at the fiber input $z = 0$, pulse width after propagation over a fiber length z can be found as follows:

$$\langle \tau^2(z) \rangle = \frac{\tau_0^2}{8} + z^2 \left[\left[\langle v_g^{-2} \rangle - \langle v_g^{-1} \rangle^2 \right] + 2 \frac{\langle D^2 \rangle}{\tau_0} \right] \quad (7)$$

where one can see the contribution of intermodal and individual mode dispersions into pulse broadening. For the calculations we assume that the initial pulse is 1 ps long.

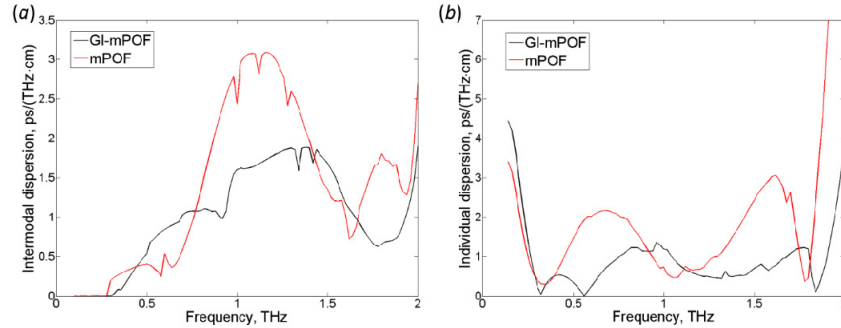


Fig. 5. (a) The individual mode dispersion and (b) the intermodal dispersion of the two fibers. The red solid lines are the dispersion properties of the proposed GI-mPOF, while the black lines show that of the traditional mPOF.

In Fig. 5, we depict the results of the computation for the two dispersion types for both the proposed GI-mPOF and the traditional mPOF. As we can see from Fig. 5, both the individual mode dispersion and the intermodal dispersion of the GI-mPOF has been reduced significantly compared to the traditional mPOF. Therefore, we expect that the proposed fiber

structure will considerably decrease the pulse width broadening by both lowering the impacts of higher order modes and by reducing intermodal dispersion.

4. THz-TDS measurement

All the measurements in our experiment were obtained by using a modified terahertz time-domain spectroscopy (THz-TDS) setup. The setup consists of a frequency doubled femtosecond fiber laser (MenloSystems C-fiber laser) used as pump source and two identical GaAs dipole antennae used as a THz emitter and a detector yielding a spectrum range of 0.1 to 3.0 THz. However, because of the lower dynamic range and increased material losses in the fiber at higher frequencies, we only considered the spectrum range of 0.2 to 1.5 THz in the following sections.

With a parabolic mirror mounted on the translation rails, our setup allows for the measurement of waveguides up to 45 cm long. Figure 6 illustrates the experimental setup where the fiber was fixed by apertures and placed between the two parabolic mirrors. To obtain the transmission properties of the fiber, we used the cutback method in the measurement. The input facet of the fiber was fixed by being glued to an aperture, while the output facet was cut in steps. Both the input and output ends of the fiber were placed at the focal points of the parabolic mirrors.

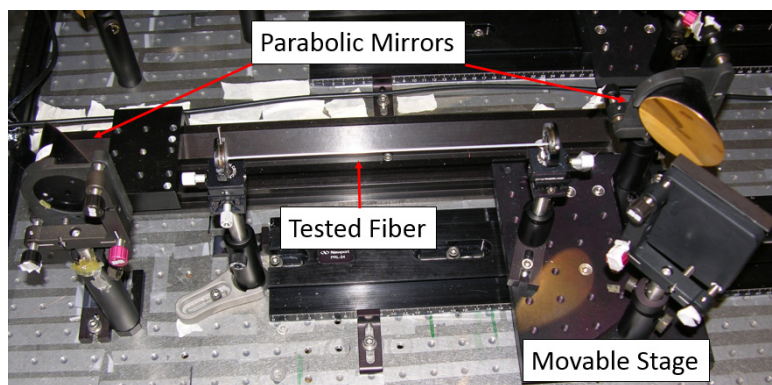


Fig. 6. Experimental setup with the fiber mounted in the apertures.

In Fig. 7, we present three temporal traces of the THz electric field measured at different fiber lengths. As expected, based on the simulations, lower intermodal dispersion of the GI-mPOF leads to the reduction of pulse broadening. With a lower difference of the group velocities, most of the modes reach the output end of the fiber in one envelope. Other higher order modes with larger mode delay were also restrained because of the low coupling coefficients. Meanwhile, in the case of the traditional mPOF, the output pulse has been separated into several groups because of the higher difference of the modal group velocities.

Another interesting phenomenon can be observed from the temporal traces of the two fibers. The output electric field of the traditional mPOF is much smaller than that of the proposed GI mPOF. This feature is caused by the weaker mode confinement of the traditional mPOF. As shown by the simulated distribution of the fundamental mode at 0.5 THz [see Fig. 7(b)], the mode of the proposed GI-mPOF is mostly concentrated in the central region of the fiber. Meanwhile, in the case of the traditional mPOF, the fundamental mode leaves the core and propagates mainly on the plastic/air interface. In our experiment, this evanescent field is blocked along with stray light by the metal aperture and partly absorbed by the glue.

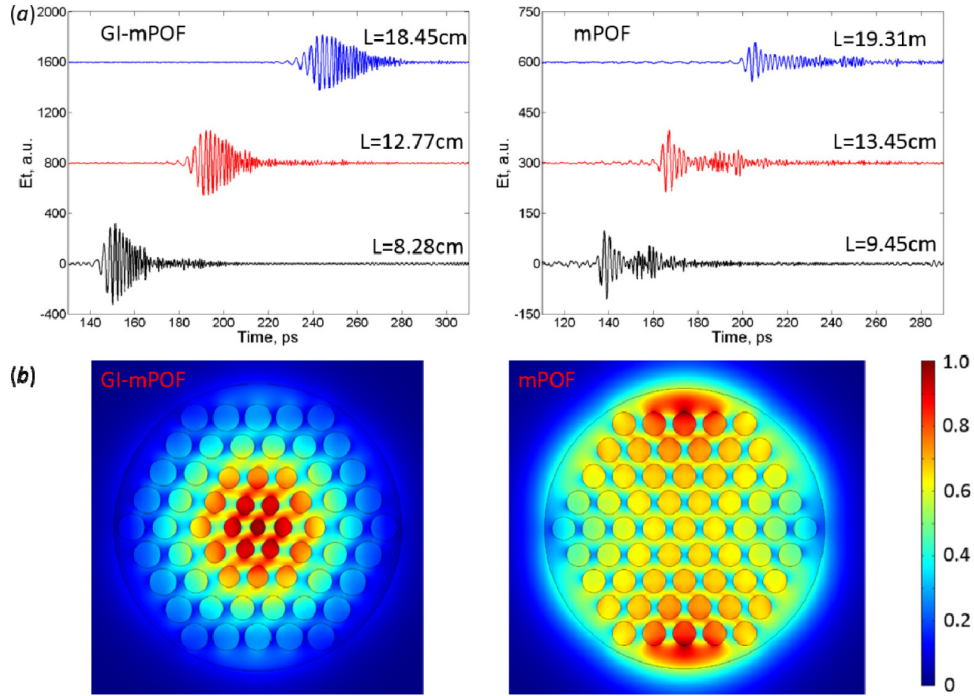


Fig. 7. (a) The time-domain traces of the THz electric field measured at different fiber lengths of the proposed GI-mPOF (left) and the traditional mPOF (right). The black trace represents the THz field after propagating a short distance in the fiber; the red trace represents a longer distance, and the blue trace is for the whole fiber. The initial lengths of the fibers used in the experiment are about 20 cm. (b) Mode profiles simulated at 0.5 THz for these two fibers.

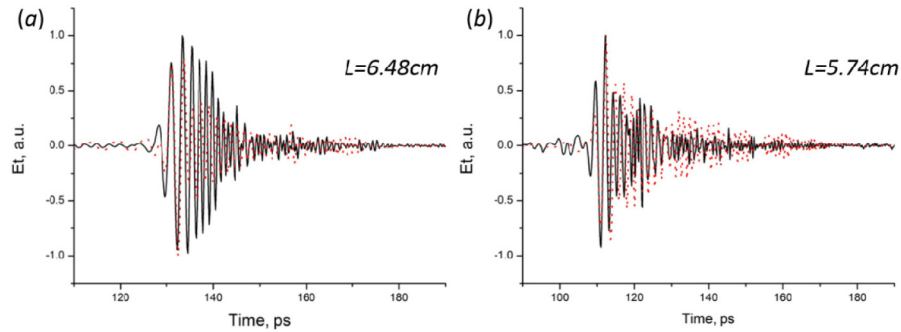


Fig. 8. The comparison between measured pulse and reconstructed pulse for (a) the GI-mPOF with 6.48 cm length and (b) the mPOF with 5.74 cm length. The black solid line represents the experimentally measured electric trace, while the red dot line corresponds to the reconstructed pulse based on the simulation results.

Because of the dispersions of the tested fiber, the input pulse with a very narrow pulse width will expand into a broader one. To investigate the pulse broadening caused by multimode propagation, we reconstructed the output pulses based on the simulation results. The reconstructed pulse at the output facet of a waveguide of length L is modeled as the inverse Fourier transform of transverse electric output field which is the coherent superposition of N guided modes where $N = 50$ for both the designed GI-mPOF and traditional mPOF.

$$\mathbf{E}(t) = \int d\omega \sum_m C_m(\omega) e^{i(\beta L - \omega t)} \iint dx dy \mathbf{E}_m(x, y, \omega) \quad (8)$$

where \mathbf{E}_m stands for the normalized transverse field components of m -th guide mode. The variable β denotes the propagation constant. In Fig. 8, we present the reconstructed pulses based on the simulation results. The experimental measured pulse of both these two fibers can be well explained by the numerical simulations. As we only considered the theoretical modal distribution here, both the coupling and launch conditions at the input ends would introduce some mismatch between the experimental and numerical results.

Using the aforementioned numerical model, we also calculated the pulse width at different propagation lengths in these fibers. In Fig. 9, we present both the experimental and theoretical values of the pulse width. The experimental values of the pulse width (dots in Fig. 9) can be found by calculating the time averages:

$$\langle \tau^2 \rangle = \langle E_t | t^2 | E_t \rangle / \langle E_t | E_t \rangle - (\langle E_t | t | E_t \rangle / \langle E_t | E_t \rangle)^2 \quad (9)$$

where E_t refers to the measured time-domain electric field trace propagating along a fiber length L . To compute the theoretical values of pulse duration, we calculated the pulse duration based on Eq. (9) where we replace the measured time-domain electric field traces by the reconstructed temporal pulses; it is depicted in Fig. 9 as solid lines. We note that for both of these two fibers, the pulse width has a L^2 dependence within some equilibrium length (L_e). Beyond this equilibrium length, the pulse width is nearly proportional to the fiber length. The value of L_e for the designed GI-mPOF is approximately 5 cm, while that of the mPOF is about 16 cm. The dashed lines in Fig. 9 are fitted using the Eq. (7) by calculation the pulse duration within L_e . The difference beyond L_e arises from the fact that the Eq. (7) is valid only for narrow bandwidth Gaussian pulses, whereas we operate with THz pulses that have very large spectral ranges. We also note that in the case of the mPOF, the weaker pulse amplitude leads to greater values of the pulse duration uncertainties as compared to that of the designed GI-mPOF.

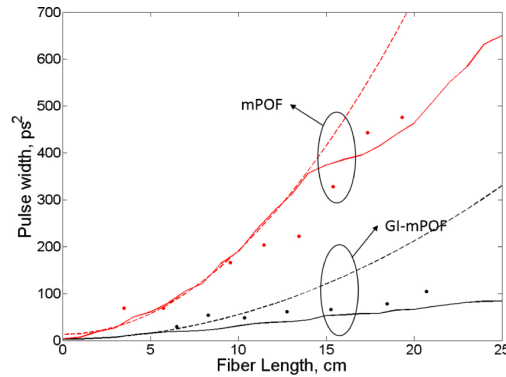


Fig. 9. The pulse duration of the designed GI-mPOF (black) and the mPOF (red). Dots - experimental results. Dashed lines - results of the fitting based on Eq. (7). Solid lines - pulse duration calculated based on the reconstructed pulses.

In Fig. 10, we present experimentally measured transmission spectra for different lengths of the GI-mPOF and mPOF corresponding to the time-domain traces shown in Fig. 7(a) and 7(b), respectively. We note that a broader transmission band from 0.2 to 1.5 THz is observed for the proposed GI-mPOF, whereas transmission merely stops at 0.8 THz and has a small peak at around 1.0 THz in the case of the traditional mPOF. Another notable feature in the measured transmission spectrum of the mPOF [Fig. 10(b)] is the amplitude fluctuation in the

higher frequency region (higher than 0.40 THz). This fluctuation is caused by the interaction of higher order modes. As shown in Fig. 4, in the case the mPOF, higher order modes occupy more modal power in the higher frequency region, thus the modal beating is more pronounced.

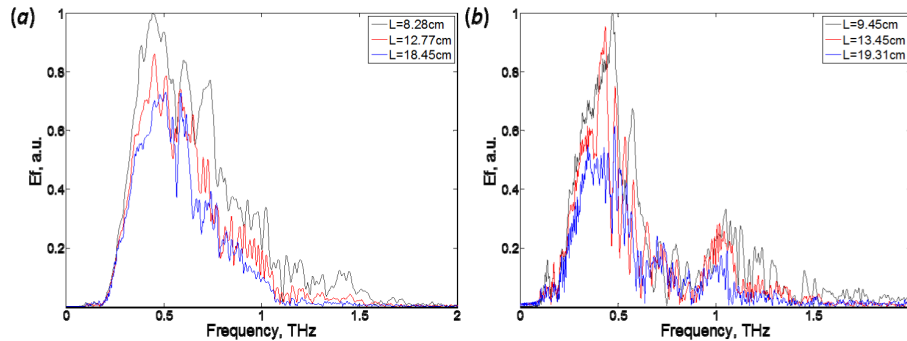


Fig. 10. Electric field amplitude as measured by the THz-TDS setup for the case of (a) GI-mPOF and (b) mPOF.

5. Conclusion

A graded index microstructured fiber designed for reducing intermodal dispersion has been proposed for applications in the THz range. The radially graded index distribution of the proposed fiber is achieved by an air-hole array featuring variable air-hole diameters and inter-hole separations. Large air holes at the outer layers of the proposed GI-mPOF lead to a better modal confinement at the center of the fiber and enhance the output electric field, as compared to the traditional mPOF with uniform air-hole diameters and lattice constants.

In this paper, we theoretically investigated the modal properties of the proposed GI-mPOF and the traditional mPOF using a finite element method. The fiber is single mode below 0.35 THz, while at higher frequencies it operates in a few-mode regime. The simulation results demonstrate that the proposed GI-mPOF design suppresses the excitation of higher order modes and reduces the intermodal dispersion. At the same time, both the intermodal and individual dispersion of the designed GI-mPOF are smaller than that of the traditional mPOF leading to a smaller broadening in the designed graded index fiber. Modal group velocity dispersions of the individual modes is reduced below 1 ps/(THz·cm) in the whole operational range due to the use of porous materials and due to the relatively large core size. At the same time, intermodal dispersion is reduced below 2 ps/(THz·cm) due to the choice of the graded index profile.

We also experimentally and numerically confirmed that the designed GI-mPOFs have considerably superior optical properties when compared to the traditional mPOF. Due to high porosity, fiber absorption loss is only a fraction of the bulk absorption loss of polyethylene, and in the whole operation range it varies from 0.025 cm⁻¹ at 0.3 THz to 0.15 cm⁻¹ at 1.5 THz. The transmission of these two fibers was also measured utilizing a THz-TDS setup using the cut-back method. According to the experimental results, the proposed fiber structure improved the output pulse quality as all the modes reach the output facet of the fiber in one time-domain envelope. We also reconstructed the output pulses based on the simulation results and calculated the pulse duration. Both the experimental and numerical results show that the pulse broadening has been well restrained by the designed fiber structure, as the pulse duration of the designed GI-mPOF is much smaller than that of the traditional mPOF, with the difference between the fibers being the most pronounced for long fiber lengths. Simultaneously, the transmission band of GI-mPOF is significantly wider than that of porous fibers due to better suppression of the excitation of higher order modes.